Inelastic processes in oxygen–hydrogen collisions

A Belyaev, Ya Voronov, A. O. Mitrushchenkov, M. Guitou, N. Feautrier

Monthly Notices
of the
ROYAL ASTRONOMICAL SOCIETY

MNRAS **487,** 5097–5105 (2019) doi:10.1093/mnras/stz1511

Inelastic processes in oxygen–hydrogen collisions

A. K. Belyaev [1]★ Ya. V. Voronov,[1] A. Mitrushchenkov,[2] M. Guitou[2] and N. Feautrier[3]

[1]*Department of Theoretical Physics and Astronomy, Herzen University, Moika 48, St Petersburg 191186, Russia*
[2]*Université Paris-Est, Laboratoire Modélisation et Simulation Multi Echelle, MSME UMR 8208, CNRS, UPEC, UPEM, 5 Bd Descartes, Champs-sur-Marne, F-77454 Marne la Vallée, France*
[3]*LERMA, Observatoire de Paris, Sorbonne University, UPMC Univ. Paris 06, CNRS-UMR 8112, F-92195 Meudon, France*

Accepted 2019 May 28. Received 2019 May 26; in original form 2019 April 30

ABSTRACT

New accurate theoretical rate coefficients for (de)-excitation and charge transfer in low-energy $O + H$, $O^+ + H^-$ and $O^- + H^+$ collisions are reported. The calculations of cross-sections and rate coefficients are performed by means of the quantum probability current method, using full configuration interaction *ab initio* electronic structure calculations that provide a global description of all 43 lowest molecular states from short to asymptotic internuclear distances. Thus, both long- and short-range non-adiabatic regions are taken into account for the first time. All the doublet, quartet and sextet OH molecular states, with excitation energy asymptotes up to 12.07 eV, as well as the two lowest ionic states with the asymptotes O^-H^+ and O^+H^- are treated. Calculations are performed for the collision energy range 0.01–100eV and the temperature range 1 000–10 000 K. The mechanisms underlying the processes are analysed: it is shown that the largest rate coefficients, with values exceeding 10^{-8} cm^3 s^{-1}, are due to ionic–covalent interactions present at large internuclear distances, while short-range interactions play an important role for rates with moderate values involved in (de)-excitation processes. As a consequence, a comparison of the present data with previously published results shows that differences of up to several orders of magnitude exist for rate coefficients with moderate values. It is worth pointing out the relatively large rate coefficients for triplet–quintuplet oxygen transitions, as well as for transitions between the $O(2p^3 3s\,^5S^o)$ and $O(2p^3 3p\,^5P)$ levels of the oxygen triplet and $H(n = 2)$ levels. The calculated data are important for modelling stellar spectra, leading to accurate oxygen abundances.

Key words: atomic data – atomic processes – scattering – stars: abundances.

1 INTRODUCTION

Oxygen is the third most important element in the Universe. Consequently, its abundance plays an important role in tracing the formation and evolution of planets, stars and galaxies (Steffen et al. 2015; Berg et al. 2016; Bertran de Lis et al. 2016; Brewer & Fischer 2016; Wilson et al. 2016; Sitnova & Mashonkina 2018). However, the value of oxygen abundance in the atmospheres of cool stars differs according to the use of different spectral diagnostics. The O I 777-nm triplet ($O(2p^3 3s\,^5S^o) \rightarrow O(2p^3 3p\,^5P)$) transition is the most commonly used for diagnostics, as the only strong feature in the spectrum, and, from comparison between observed spectra and models, it can be seen clearly that the O I 777-nm triplet transition lines are not formed under the local thermodynamic equilibrium (LTE) assumption (Steffen et al. 2015; Pazira, Kiselman & Leenaarts 2017; Amarsi et al. 2018; Sitnova & Mashonkina 2018). For the Sun and cool stars, the main inaccuracy in non-LTE models lies in the lack of excitation and ion pair production collision rates with neutral hydrogen (Sitnova & Mashonkina 2018), as well as their inverse processes: de-excitation and mutual neutralization.

Several non-LTE studies of oxygen stellar spectra have been performed (Allende Prieto, Asplund & Fabiani Bendicho 2004; Pereira, Asplund & Kiselman 2009; Steffen et al. 2015) using the Drawin formula (Drawin 1968, 1969; Steenbock & Holweger 1984) for H collisional rate coefficients with a scaling factor S_H adjusted to improve the fit of the lines. However, from comparisons with full quantum calculations for several elements, including Li, Na and Mg atoms (Belyaev et al. 1999, 2010, 2012; Belyaev & Barklem 2003; Guitou et al. 2011), it was shown that the Drawin recipe, based on the classical formula for ionization by electron impact, fails to describe the underlying mechanisms existing in inelastic collisions with hydrogen (Barklem et al. 2011), as it is well established that inelastic transitions occur in regions of avoided crossings associated with ionic–covalent or covalent–covalent interactions between H and the studied atom. This requires accurate quantum calculations

★ E-mail: andrey.k.belyaev@gmail.com

of molecular interactions for all internuclear distances, as well as a good description of the scattering processes.

In the absence of quantum data, an asymptotic semi-empirical model approach (Belyaev 2013a) for the electronic structure, combined with the Landau–Zener model for nuclear dynamics, has been proposed to obtain transition rate coefficients. This approach has two versions: (i) the multichannel Landau–Zener approach (Yakovleva, Voronov & Belyaev 2016, see also references therein), which takes into account multiple ionic–covalent interactions at large distances, and (ii) the more accurate branching probability current method (Belyaev 2013a), which includes non-adiabatic transitions at all distances. These approaches, which have been applied to H collisions with Al (Belyaev 2013b), Si (Belyaev, Yakovleva & Barklem 2014), Mg (Guitou et al. 2015), Be (Yakovleva et al. 2016), Ca (Belyaev et al. 2017; Mitrushchenkov et al. 2017), K and Rb (Yakovleva, Barklem & Belyaev 2018a), Ba and Ba^+ (Belyaev & Yakovleva 2018), and Fe and Fe^+ (Yakovleva, Belyaev & Kraemer 2018b, 2019) atoms and ions, are expected to provide reliable estimates for cross-sections and rate coefficients with large values. Recently, the asymptotic Linear Combinations of Atomic Orbitals (LCAO) method was proposed by Barklem (2016, 2017) to obtain long-range non-adiabatic regions. Comparisons of the results for the cases of K–H, Rb–H and Ca–H collisions show that the asymptotic semi-empirical and LCAO models perform roughly equally well, on average, for large rate coefficients (Belyaev et al. 2017; Yakovleva et al. 2018a). However, it is important to notice that short-range avoided crossings, not described in the asymptotic approaches, may open mechanisms that contribute substantially to processes with lower values.

The O–H case is more complicated than the previously studied systems, as two ionic states dissociating towards O^-–H^+ and O^+–H^- contribute to the collisional processes. In the past, many experimental (de Beer et al. 1991; Greenslade et al. 2005; Beames et al. 2011) and theoretical (Easson & Pryce 1973; van Dishoeck, Langhoff & Dalgarno 1983; Stephens & McKoy 1990; van der Loo & Groenenboom 2005; Li et al. 2012; Qin & Zhang 2014) studies have been devoted to OH. However, all these works imply the determination of the energies at short O–H distances, while scattering calculations need data at all internuclear distances *R*. Recently, long-range OH potentials were calculated by the asymptotic LCAO method for a number of molecular symmetries (Barklem 2018). Very recently, *ab initio* electronic structure calculations were performed by Mitrushchenkov et al. (2019) for all O–H molecular states up to the $O(2p^3 4s\,^3S^o) + H(1s)$ asymptote, plus the lowest $^2\Sigma^+$, $^2\Pi$ and $^4\Sigma^-$ molecular states associated with the O^-–H^+ and O^+–H^- ionic states, respectively. Full configuration interaction (CI) calculations were carried out with a very small *R* step size in order to describe the avoided crossings accurately at all internuclear distances. These data, combined with dynamical calculations performed using the hopping probability current method (Belyaev 2013a), are reported in the present article.

2 BRIEF THEORY

2.1 Ab initio adiabatic potentials

Ab initio calculation of the interaction energies for a large number of molecular states from small to large internuclear distances *R* is very challenging using the usual IC-MRCI (the Internally Contracted Multi-Reference Configuration Interaction method) calculations, due to the very large number of orbitals needed to describe the colliding system correctly at all distances. Full CI calculations are therefore performed; these avoid the orbital jumps present in the IC-MRCI calculations of excited states when electronic states not taken explicitly into account appear, leading to discontinuities in the potentials (Mitrushchenkov et al. 2019). These calculations are based on Efficient Configuration Interaction (ECI), an Efficient Configuration Interaction code that is a modified version of the Dynamic CI code (Mitrushenkov 1994). Table 1 presents a list of the symmetries of the calculated molecular states and their asymptotic scattering channels, as well as their asymptotic energies; see also Table A1 in Appendix A for the statistical probabilities of the scattering channels. 20 doublet states, 19 quartet states and four sextet states were considered and the corresponding potentials were calculated with a very small *R* step size, in order to describe the avoided crossings accurately. These molecular states are expected to provide a major contribution to O–H collision processes. Channels 1–11 give the asymptotic states involving O and H excited states, while channels *i*1 and *i*2 describe the O^-–H^+ and O^+–H^- ionic channels, respectively. Contributions to collisional processes from higher states, dissociating to the $O(2p^3 3d\,^5D^o) + H(1s)$, $O(2p^3 3d\,^3D^o) + H(1s)$ and $O(2p^4\,^3P) + H(3s, p, d)$ asymptotes, are expected to be much smaller, as crossings occur at very large distances, leading to a quasi-diabatic collision mechanism. The calculations do not take spin-orbit couplings into account.

Table 1. Scattering channels, corresponding molecular states and asymptotic energies, taken from *ab initio* calculations (Mitrushchenkov et al. 2019).

j	Scattering channels	Molecular states	Asymptotic energies (eV)
1	$O(2p^4\,^3P) + H(1s)$	$^2\Sigma^-$, $^2\Pi$, $^4\Sigma^-$, $^4\Pi$	0
2	$O(2p^4\,^1D) + H(1s)$	$^2\Sigma^+$, $^2\Pi$, $^2\Delta$	2.05
3	$O(2p^4\,^1S) + H(1s)$	$^2\Sigma^+$	4.69
4	$O(2p^3 3s\,^5S^o) + H(1s)$	$^4\Sigma^-$, $^6\Sigma^-$	9.16
5	$O(2p^3 3s\,^3S^o) + H(1s)$	$^2\Sigma^-$, $^4\Sigma^-$	9.59
6	$O(2p^4\,^3P) + H(2s)$	$^2\Sigma^-$, $^2\Pi$, $^4\Sigma^-$, $^4\Pi$	10.20
7	$O(2p^4\,^3P) + H(2p)$	$^2\Sigma^+$, $^2\Sigma^-(\times 2)$, $^2\Pi(\times 2)$, $^2\Delta$ $^4\Sigma^+$, $^4\Sigma^-(\times 2)$, $^4\Pi(\times 2)$, $^4\Delta$	10.27
8	$O(2p^3 3p\,^5P) + H(1s)$	$^4\Sigma^-$, $^4\Pi$, $^6\Sigma^-$, $^6\Pi$	10.82
9	$O(2p^3 3p\,^3P) + H(1s)$	$^2\Sigma^-$, $^2\Pi$, $^4\Sigma^-$, $^4\Pi$	11.07
10	$O(2p^3 4s\,^5S^o) + H(1s)$	$^4\Sigma^-$, $^6\Sigma^-$	11.93
11	$O(2p^3 4s\,^3S^o) + H(1s)$	$^2\Sigma^-$, $^4\Sigma^-$	12.07
*i*1	$O^-(2p^5\,^2P) + H^+$	$^2\Sigma^+$, $^2\Pi$	12.39
*i*2	$O^+(2p^3\,^4S^o) + H^-(^1S)$	$^4\Sigma^-$	12.90

The most important adiabatic potentials are displayed in the following figures. Figs 1 and 2 show the OH potentials for the $^2\Sigma^+$ and $^2\Pi$ symmetries as functions of the internuclear separation. One observes many interactions between consecutive states, particularly with long-range avoided crossings that correspond to exchange between the ionic O^-–H^+ configuration and the neutral O–H configurations. Fig. 3 presents the 11 adiabatic $OH(^4\Sigma^-)$ potential energies, including the ionic O^+–H^- potential. A series of long-range avoided crossing regions due to ionic–covalent interactions is clearly seen. In addition, one can see many non-adiabatic regions at intermediate and short distances. It is worth emphasizing that the long-range non-adiabatic regions created by the ground ionic states interacting with covalent states exist only in the $^2\Sigma^+$ and $^2\Pi$ molecular symmetries (for the ionic O^-–H^+ configuration) and in the $^4\Sigma^-$ symmetry (for the O^+–H^- configuration). It is also seen that, within these molecular symmetries, avoided crossings occur at shorter internuclear distances. Similar avoided crossings

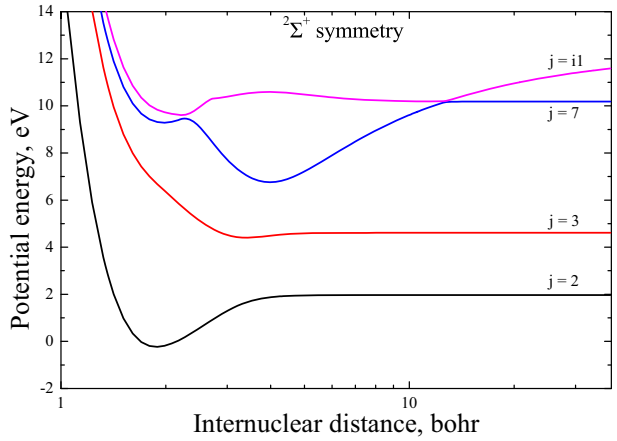

Figure 1. Adiabatic potentials of the OH($^2\Sigma^+$) states including the potential for the ground-state ionic O^-–H^+ configuration ($i1$) as functions of the internuclear distance.

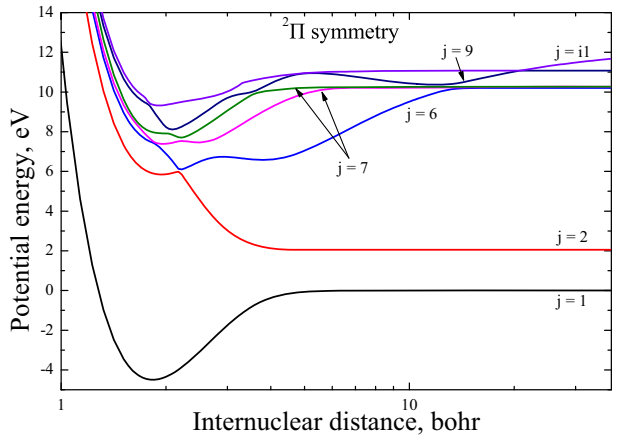

Figure 2. Adiabatic potentials of the OH($^2\Pi$) states including the potential for the ground-state ionic O^- – H^+ configuration ($i1$) as functions of the internuclear distance.

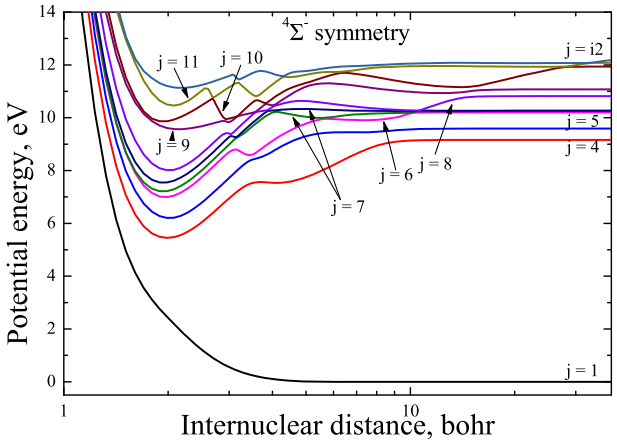

Figure 3. Adiabatic potential energies of the OH($^4\Sigma^-$) states including the potential for the ground-state ionic O^+ – H^- configuration ($i2$) as functions of the internuclear distance.

are present in other symmetries that do not have ground-state ionic configurations, e.g. the $^2\Sigma^-$, $^4\Pi$ and $^2\Delta$ symmetries (see Mitrushchenkov et al. 2019).

2.2 Non-adiabatic nuclear dynamics

In the present work, non-adiabatic nuclear dynamics calculations are performed by means of the hopping probability current method (Belyaev 2013a) based on accurate *ab initio* adiabatic potentials (Mitrushchenkov et al. 2019). The advantage of the probability current method is that it takes both long- and short-range non-adiabatic regions into account.

The probability current method treats an inelastic collision problem within the Born–Oppenheimer approach, which divides the problem into two parts: (i) a fixed-nuclei electronic structure calculation and (ii) a non-adiabatic nuclear dynamical calculation. The electronic structure calculation has been accomplished by the full CI approach (see Mitrushchenkov et al. 2019 and references therein). The OH adiabatic potentials have been computed (see Figs 1–3 above and Mitrushchenkov et al. 2019). The calculated potentials allow us to treat the non-adiabatic nuclear dynamics.

For a given collision energy E and total angular momentum quantum number J, the probability current method treats the evolution of incoming and outgoing probability currents of a considered collision system as functions of an internuclear distance with proper boundary conditions in the asymptotic region. These boundary conditions are set for incoming currents to be unity for one channel i and zero for other channels. During the evolution, the incoming and outgoing currents pass different non-adiabatic regions, where non-adiabatic transitions occur. The probability current method evaluates these transition probabilities by means of an adiabatic-potential-based formula (Belyaev & Lebedev 2011) within the Landau–Zener model. Finally, outgoing probability currents in the asymptotic region after a collision determine inelastic state-to-state transition probabilities for all scattering channels. In the present work, we use the probabilistic version of the hopping probability current method (see Belyaev, Voronov & Gadéa 2018 for details). Comparison of the data obtained by the probability current method and by the full quantum calculation for $Li^+ + H^-$ collisions shows good agreement (see Belyaev & Voronov 2018). State-to-state transition probabilities allow us to calculate inelastic cross-sections and rate coefficients. The rate coefficients for exothermic processes depend weakly on the temperature (see Section 3, Fig. 10 as an example). To take this into account and to avoid energy threshold effects, the rate coefficients are first calculated for mutual neutralization and de-excitation processes and the rate coefficients for the reverse processes are obtained by means of the detailed balance relationship.

3 O + H, $O^+ + H^-$, $O^- + H^+$ COLLISIONS

Inelastic $O + H$, $O^+ + H^-$ and $O^- + H^+$ collisions are studied in the present work by means of the hopping probability current method based on accurate *ab initio* potentials (Mitrushchenkov et al. 2019), as described briefly in the previous section. The calculated rate coefficients for transitions between the channels listed in Table 1 are presented in the supplementary materials for the temperature range $T = 1000$–$10\,000$ K. Table 2 gives an example of the calculated rates at $T = 6000$ K. A graphical representation of the data from this table is plotted in Fig. 4.

It is seen from Table 2 and Fig. 4 that the highest rates with values exceeding 10^{-8} cm^3 s^{-1} correspond to mutual neutralization

Table 2. Rate coefficients (in units of $cm^3\ s^{-1}$) summed over all considered molecular symmetries for inelastic partial processes between the states collected in Table 1 at temperature $T = 6000$ K.

	1	2	3	4	5	6	7	8	9	10	11	i1	i2
1	–	0.00e + 00	0.00e + 00	0.00e + 00	0.00e + 00	9.97e−20	1.04e−19	1.53e−20	3.81e−22	0.00e + 00	0.00e + 00	0.00e + 00	0.00e + 00
2	0.00e + 00	–	5.04e−27	0.00e + 00	0.00e + 00	1.07e−17	1.56e−17	0.00e + 00	7.62e−19	0.00e + 00	0.00e + 00	5.78e−20	0.00e + 00
3	0.00e + 00	1.85e−24	–	0.00e + 00	0.00e + 00	0.00e + 00	5.87e−19	0.00e + 00	0.00e + 00	0.00e + 00	0.00e + 00	1.14e−19	0.00e + 00
4	0.00e + 00	0.00e + 00	0.00e + 00	–	1.08e−11	6.84e−12	1.14e−12	1.25e−13	1.44e−15	2.07e−17	1.59e−17	0.00e + 00	6.49e−17
5	0.00e + 00	0.00e + 00	0.00e + 00	3.72e−11	–	2.14e−10	4.90e−11	1.11e−11	1.81e−11	6.28e−12	6.91e−13	0.00e + 00	2.78e−13
6	3.68e−11	4.88e−11	0.00e + 00	2.92e−11	2.65e−10	–	4.42e−09	7.54e−11	4.70e−11	1.17e−12	2.54e−12	1.51e−11	5.32e−13
7	1.28e−11	2.38e−11	2.43e−15	1.61e−12	2.03e−11	1.47e−09	–	2.84e−11	3.40e−11	1.16e−12	3.69e−12	6.55e−11	6.15e−13
8	9.66e−12	0.00e + 00	0.00e + 00	9.13e−13	2.34e−11	1.29e−10	1.45e−10	–	1.02e−10	6.17e−12	2.22e−12	0.00e + 00	3.80e−12
9	6.48e−13	1.60e−11	0.00e + 00	2.82e−14	1.03e−10	2.16e−10	4.69e−10	2.74e−10	–	1.50e−10	3.29e−11	1.43e−11	1.17e−10
10	0.00e + 00	0.00e + 00	0.00e + 00	3.77e−15	3.32e−10	4.98e−11	1.49e−10	1.54e−10	1.39e−09	–	5.98e−10	0.00e + 00	1.62e−09
11	0.00e + 00	0.00e + 00	0.00e + 00	5.79e−15	7.30e−11	2.16e−10	9.42e−10	1.11e−10	6.09e−10	1.19e−09	–	0.00e + 00	9.30e−10
i1	0.00e + 00	3.45e−11	1.84e−13	0.00e + 00	0.00e + 00	1.97e−09	2.56e−08	0.00e + 00	4.06e−10	0.00e + 00	0.00e + 00	–	0.00e + 00
i2	0.00e + 00	0.00e + 00	0.00e + 00	2.15e−13	2.68e−10	4.14e−10	1.44e−09	1.73e−09	1.98e−08	2.95e−08	8.48e−09	0.00e + 00	–

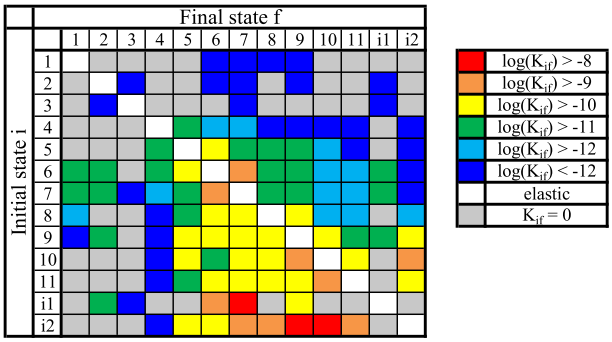

Figure 4. Graphical representation of the rate coefficients (in units of $cm^3\ s^{-1}$, summed over all considered molecular symmetries) for mutual neutralization, ion-pair formation, excitation and de-excitation processes in oxygen–hydrogen collisions for temperature $T = 6000$ K.

processes. In particular, one can see that at $T = 6000$ K the highest rate coefficient is equal to 2.95×10^{-8} $cm^3\ s^{-1}$ for the partial mutual neutralization process $O^+ + H^- \rightarrow O(2p^3 4s\ ^5S^o) + H(1s)$ (the $i2 \rightarrow 10$ transition). The second largest rate, with the value 2.56×10^{-8} $cm^3\ s^{-1}$, corresponds to the partial neutralization $O^- + H^+ \rightarrow O(2p^4\ ^3P) + H(2p)$ (the $i1 \rightarrow 7$ transition; note the different ionic channels and molecular symmetries). The third largest rate coefficient has the value 1.98×10^{-8} $cm^3\ s^{-1}$ and corresponds to the mutual neutralization process $O^+ + H^- \rightarrow O(2p^3 3p\ ^3P) + H(1s)$ (the $i2 \rightarrow 9$ transition). These three partial processes belong to the so-called most 'optimal window',[1] in accordance with the general finding of the simplified model (Belyaev & Yakovleva 2017), which predicts the largest rates for mutual neutralization processes with final-state binding energies in the vicinity of –2 eV. This 'optimal window' is well understood through the Landau–Zener model, which describes inelastic atomic collision processes due to long-range non-adiabatic regions created by ionic–covalent interactions. Rate coefficients for the inverse processes, ion-pair production, also have substantial values, up to and exceeding 10^{-9} $cm^3\ s^{-1}$. These processes belong to the group of processes with moderate rate coefficients with values between 10^{-10} and 10^{-8} $cm^3\ s^{-1}$. Many mutual neutralization processes in both $O^+ + H^-$ and $O^- + H^+$ collisions belong to this group; see Table 2 and Fig. 4.

The rate coefficients for the (de-)excitation processes have values that are at least an order of magnitude lower than the maximal values for neutralization: the maximum (de-)excitation rates slightly exceed the value 10^{-9} $cm^3\ s^{-1}$, while the rates correspond to the transitions $6 \leftrightharpoons 7$, $10 \rightarrow 9$, $11 \rightarrow 10$. Note that the scattering channels 6 and 7 correspond to participation of excited hydrogen states H(2s) and H(2p). These processes, as well as many other (de-)excitation processes with rate values exceeding 10^{-10} $cm^3\ s^{-1}$, belong to the group of processes with moderate rate coefficients. Processes from the first two groups are expected to be important for non-LTE stellar atmosphere modelling.

Other processes with low rate coefficients, lower than 10^{-10} $cm^3\ s^{-1}$, belong to a third group. These processes are expected to be less important for non-LTE modelling; nevertheless it is worth estimating low-valued rate coefficients reliably in order to calculate populations for particular states of interest.

[1]By an 'optimal window', we mean an atomic binding-energy range such that scattering channels located into this range have large-valued rate coefficients.

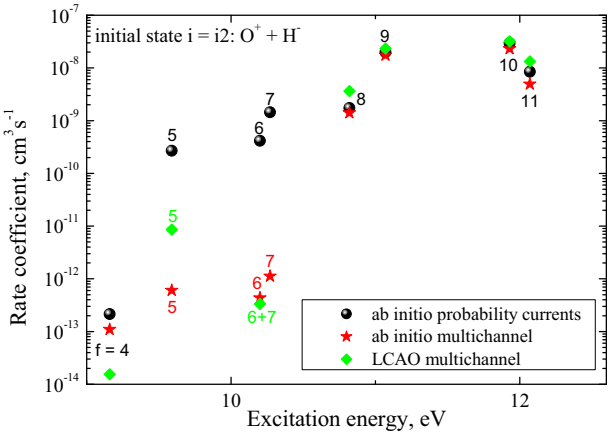

Figure 5. Rate coefficients for mutual neutralization processes in $O^+ + H^-$ collisions for the $^4\Sigma^-$ molecular symmetry at temperature $T = 6000$ K as a function of the final channel excitation energy. Circles depict the results of the present calculation by the probability current method based on *ab initio* potentials (Mitrushchenkov et al. 2019), stars the results of the multichannel approach based on *ab initio* potentials (Mitrushchenkov et al. 2019) and rhombuses the results of the multichannel approach based on asymptotic LCAO potentials (Barklem 2018).

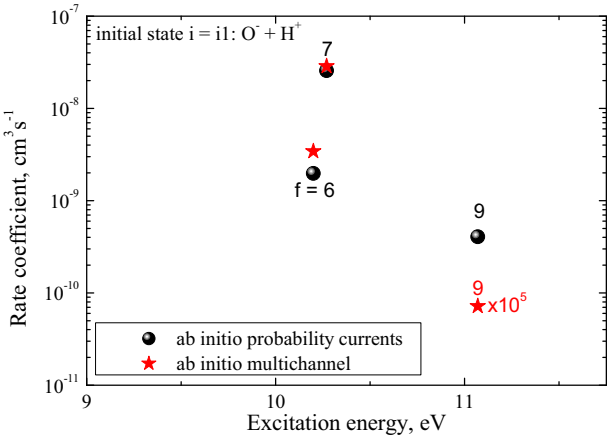

Figure 6. Rate coefficients for mutual neutralization processes in $O^- + H^+$ collisions for the $^2\Sigma^+$ and $^2\Pi$ molecular symmetries at temperature $T = 6000$ K as a function of the final channel excitation energy. Symbols are as described in Fig. 5; note the different initial ionic channel. Note also that the multichannel rate coefficient for the $i1 \rightarrow 9$ transition process is multiplied by a factor of 10^5.

The important features are the distributions of rate coefficients between the final channels for a given initial channel. Fig. 5 shows such a distribution for the initial ionic channel $O^+ + H^-$ of the mutual neutralization processes $i = i2 \rightarrow f$ (the present calculations are shown by black circles). One can see that the rate coefficients decrease in both directions as the excitation energies of the final channels move outside the most optimal window in both directions: above 12 eV and below 11 eV at present. Two final channels, $f = 10$ and $f = 9$, belong to the most optimal window. Fig. 6 displays a similar distribution for another ionic channel $O^- + H^+$ of the mutual neutralization processes $i = i1 \rightarrow f$. Here only one partial process, $i = i1 \rightarrow f = 7$, belongs to the optimal window. Note that optimal windows have different excitation energy ranges for different initial channels, $i1$ and $i2$ at present. For excitation and de-excitation processes, an example of the distribution is shown

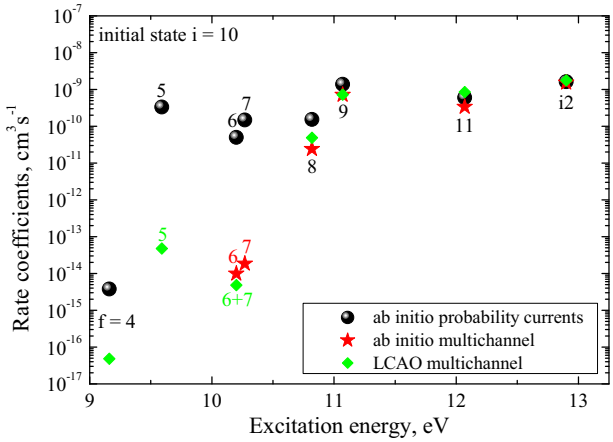

Figure 7. Rate coefficients of excitation, de-excitation and ion-pair production processes summed up over transitions in different molecular symmetries for the initial channel $i = 10$ at temperature $T = 6000$ K as a function of the final-channel excitation energy. Symbols are as described in Fig. 5.

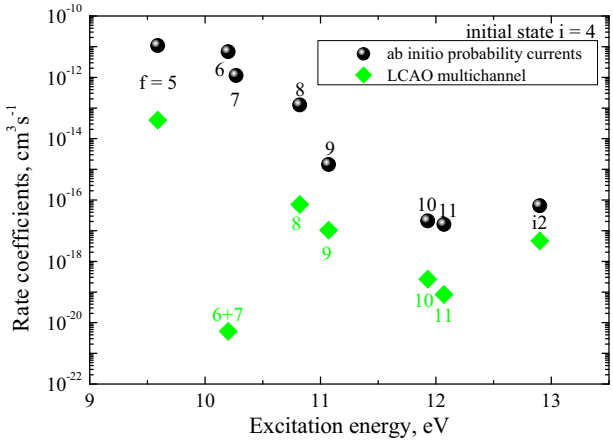

Figure 8. Rate coefficients of excitation, de-excitation and ion-pair production processes summed up over transitions in different molecular symmetries for initial channel $i = 4$ at temperature $T = 6000$ K as a function of the final-channel excitation energy. Symbols are as described in Fig. 5.

in Fig. 7 for the initial channel $i = 10$. Note that the transition $10 \rightarrow 9$ has one of the largest rate coefficients. For these high-lying levels, the distribution for the (de-)excitation processes is similar to that for the neutralization processes as dominated by long-range interactions, though the decreases are not so steep. It is worth emphasizing that scattering channels exist in the range between the covalent channel $f = 11$ and the ionic channels $i1$ or $i2$. Their contribution is expected to be small, as the colliding system passes the corresponding avoided crossings almost diabatically. Excitation and de-excitation processes involving low-lying states are sensitive to short-range avoided crossings, correctly accounted for by the probability current method based on accurate *ab initio* potentials.

As mentioned above, the oxygen triplet transition $4 \leftrightharpoons 8$ is of particular astrophysical interest. For this reason, partial processes to and from these states are of special interest. Figs 8 and 9 therefore show the distributions of inelastic processes from the initial channels $i = 4$ and $i = 8$, respectively. It is seen that the rates from channel 4 have low values, 10^{-11} cm^3 s^{-1} as a maximum, as well as the rates for all transitions between low-lying states (see Table 2), and that the rates decrease with increasing excitation energies.

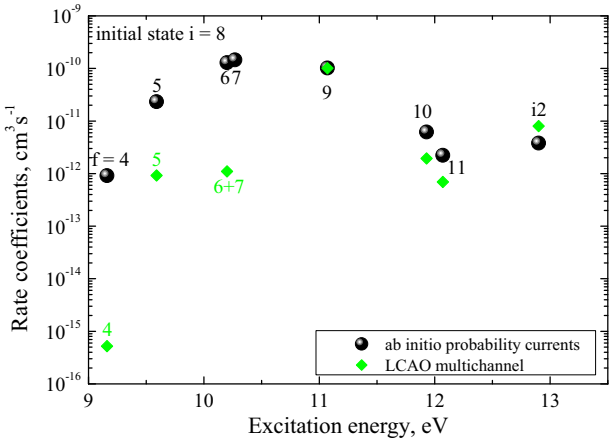

Figure 9. Rate coefficients of excitation, de-excitation and ion-pair production processes summed up over transitions in different molecular symmetries for initial channel $i = 8$ at temperature $T = 6000$ K as a function of the final-channel excitation energy. Symbols are as described in Fig. 5.

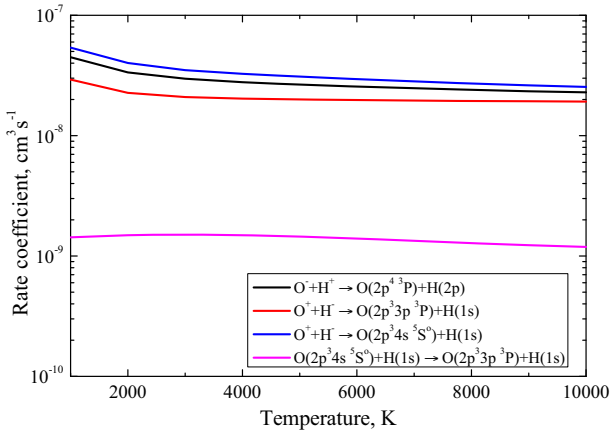

Figure 10. Rate coefficients for some neutralization and de-excitation processes as a function of temperature.

For initial channel $i = 8$, the maximum rates are higher, up to 1.45×10^{-10} cm^3 s^{-1} for the final channel $f = 7$. The rate coefficients then decrease for transitions involving more distant levels. Deviation of the excitation energy from the optimal value in both directions results in a decrease of the (de-)excitation rate coefficients. It is important to mention the relatively large rate coefficients, which rely on the two oxygen levels 8 and 9 with the $n = 2$ excited levels of hydrogen (channels 6 and 7). Finally, it is important to note the existence of relatively large-valued rate coefficients for the transitions between triplet and quintuplet states of oxygen due to H collisions.

It is worth mentioning that the data presented in Table 2 and Figs 4–9 are obtained as sums over different molecular symmetries. In particular, for scattering channel 4 (O(2p^{3}3s ^{5}S^o) + H(1s)) there are two symmetries, $^4\Sigma^-$ and $^6\Sigma^-$, which could contribute in the processes (see Table 1), but in fact the rates in the symmetry $^6\Sigma^-$ are at least six orders of magnitude lower than in the symmetry $^4\Sigma^-$, so in practice the transitions in the symmetry $^4\Sigma^-$ determine the rate coefficients involving channel 4. For scattering channel 8 (O(2p^{3}3p ^{5}P) + H(1s)), the situation is different: transitions in the $^4\Sigma^-$ symmetry are also dominant, but contributions from other symmetries, first of all $^4\Pi$, are comparable with those from the $^4\Sigma^-$ symmetry up to roughly 40 per cent. Thus, it is important to take transitions in all the different molecular symmetries into account, and this is done in the present work.

It is also worth mentioning that rate coefficients for neutralization and de-excitation processes, that is, exothermic processes, depend weakly on the temperature – see Fig. 10 as an example – while rates for their inverse processes, ion pair production and excitation, exhibit a strong dependence due to the balance equation. For this reason, it is better to analyse and compare rate coefficients for exothermic processes than for endothermic ones.

Let us now compare our results with other available data and discuss the accuracy of the calculations. Krems, Jamieson & Dalgarno (2006) have calculated the O(^{1}D → ^{3}P) relaxation rate coefficient in collisions with H based on the accurate potentials from Parlant & Yarkony (1999). They took spin-orbit and rotational couplings into account in the coupled-channel equations and found the relaxation rate coefficient to be of magnitude 10^{-12} cm^3 s^{-1} in the temperature range 1 000–10 000 K. This study shows that the spin-orbit coupling plays a major role for transitions involving the O(2p^4 ^{3}P) oxygen ground state, the effect of the rotational coupling being less important, although not negligible. This relaxation rate agrees within a factor of 1.5 with the value obtained by Federman & Shipsey (1983) by means of the Landau–Zener model calculation. Later on, Abrahamsson, Krems & Dalgarno (2007) calculated the ground-state fine-structure excitation of O by impact with atomic hydrogen. Though the excitation rates are not negligible, up to and above 10^{-10} cm^3 s^{-1}, fine-structure transitions are outside the scope of the present article. The present calculations give a zero rate for the O(^{1}D → ^{3}P) relaxation, because they do not include spin-orbit couplings and the corresponding potentials do not exhibit any avoided crossing (see Fig. 2). In any case, the quantum calculations of Krems et al. (2006) found this relaxation rate to be relatively low. We note that, in the case of Na + H (Belyaev et al. 1999) and Mg + H collisions (Guitou et al. 2011), rotational couplings were also found to give small contributions at the temperatures involved in stellar applications. Spin-orbit and rotational couplings are not taken into account in the present study.

Recently, the rate coefficients for inelastic processes in O + H and O$^+$ + H$^-$ collisions have been calculated by Barklem (2018) by means of a multichannel approach based on the asymptotic LCAO potentials. Let us discuss the accuracy of these calculations compared with the present calculations, as well as with the multichannel calculation based on the *ab initio* potentials. All three calculations are performed within the Born–Oppenheimer approach, which divides a collision problem into an electronic structure calculation and a non-adiabatic nuclear dynamical one. Considering first the electronic structure data, the *ab initio* full CI electronic structure calculations (Mitrushchenkov et al. 2019) have the highest global accuracy, as they describe the potentials from short to large internuclear distances. The variational character of this *ab initio* approach is expected to describe the shape of the potentials around the avoided crossings accurately, which is of crucial importance for dynamics applications. However, the agreement between calculated and experimental asymptotic energies is not perfect for all states (differences are found within a few 10^{-2} eV); this could lead to some uncertainties in the rate coefficients at low temperatures. Obviously, taking the experimental asymptotic energies as input, the LCAO approach does not have such uncertainties at large distances.

The nuclear dynamics in all three calculations are treated using the Landau–Zener model. Rotational and fine-structure couplings are neglected in all three approaches, but the multichannel approach takes into account only long-range non-adiabatic regions, while

the probability current method accounts for all regions. Thus, the present data obtained by means of the *ab initio* probability current calculations could be considered as the most accurate to date. Then follow the data computed by the *ab initio* multichannel formulae, since short-range non-adiabatic regions are not taken into account. It is worth mentioning the simplified model (Belyaev & Yakovleva 2017) among the quantum model approaches. Although the simplified model is expected to have the lowest accuracy, it estimates quite reliable large- and moderate-valued rate coefficients for inelastic processes in collisions with hydrogen.

Comparison of the LCAO multichannel results with the present *ab initio* current results, as well as the *ab initio* multichannel ones, is depicted in Figs 5–9. For mutual neutralization in $O^+ + H^-$ collisions, the comparison is shown in Fig. 5. It is seen that the asymptotic LCAO multichannel approach (Barklem 2018) agrees well with the present *ab initio* probability current method for the largest rate coefficients (final channels $f = 9$–11). Comparison of the present data with the *ab initio* multichannel calculation shows the same agreement. However, both multichannel approaches underestimate the rates for other partial processes with low rate coefficients, typically by several orders of magnitude (final channels $f = 4$–7).

Analysis shows that neutralization into final channels $f = 9$–11 is determined by the long-range avoided crossings and is probably not so sensitive to variation of the Landau–Zener parameters, while in neutralization into final channels $f = 4$–7 the collisional processes are due to interactions in the short-range regions and are sensitive to the Landau–Zener parameters. Unfortunately, it is not possible to compare neutralization rates in $O^- + H^+$ collisions (Fig. 6), since these collisions are not treated in Barklem (2018).

The conclusion for excitation and de-excitation processes is similar to one made for neutralization processes. As previously stated by Barklem (2018), the LCAO multichannel approach cannot describe short-range interactions correctly. The LCAO multichannel data are typically underestimated (up to several orders of magnitude) compared with the present *ab initio* probability current data, except for partial processes with large-valued rate coefficients (see Figs 7–9). The same conclusion is found for multichannel data obtained from calculations based on the *ab initio* potentials.

It is interesting that applications of LCAO multichannel data (Barklem 2018) to non-LTE modelling (Pazira et al. 2017; Amarsi et al. 2018) led to the same conclusion: that the LCAO multichannel data are underestimated when long-range ionic–covalent interactions are not dominant and more accurate calculations are very important. Such, more accurate, data are revealed by the present work.

4 CONCLUSIONS

The partial cross-sections and rate coefficients in low-energy O + H, $O^+ + H^-$ and $O^- + H^+$ collisions are calculated for all transitions involving the O–H molecular states up to the $O(2p^3 4s\ ^3S^o) + H(1s)$ asymptote, plus the lowest $^2\Sigma^+$, $^2\Pi$ and $^4\Sigma^-$ molecular states associated with the $O^- - H^+$ and $O^+ - H^-$ ionic state asymptotes, respectively. The non-adiabatic nuclear dynamics of the O + H collisional system is studied by means of the probability current method based on accurate *ab initio* adiabatic potentials (Mitrushchenkov et al. 2019). This approach allows us to take both long- and short-range non-adiabatic regions into account. All 43 doublet, quartet and sextet OH molecular states are taken into account for a collision energy range from 0.01–100 eV and temperature range from 1 000–10 000 K. The calculated rate coefficients are available online as supplementary material to the present article.

The present study selects partial inelastic processes with high and moderate values of the rate coefficients. It is found that the reaction mechanism for processes with high-valued rates is due to long-range ionic–covalent interaction, while for processes with smaller rates short-range interactions play an important role. It is also important to mention that although the $^2\Sigma^+$, $^2\Pi$ and $^4\Sigma^-$ molecular states, associated with ionic configurations, have the dominant contribution for many channels, other molecular symmetries (such as $^4\Pi$) give significant contributions and should be taken into account. In accordance with the predictions of the simplified model (Belyaev & Yakovleva 2017), the distribution of the rate coefficients between different final channels for a given initial channel exhibits a maximum due to long-range ionic–covalent interactions and decreases in both directions from this value.

All partial processes can be divided into three groups according to the value of their rate coefficients. It is found that the highest rates with values exceeding 10^{-8} cm^3s^{-1} correspond to mutual neutralization processes from $O^+ + H^-$ and $O^- + H^+$. Rate coefficients for the inverse processes also have high-valued rate coefficients, up to 10^{-9} cm^3s^{-1}. Rate coefficients for (de)-excitation processes have smaller values (between 10^{-8} and 10^{-10} cm^3s^{-1}). It is important to point out the relatively large H-collisional rate coefficients found for processes with initial as well as final quintuplet levels of oxygen with oxygen triplet states and with the excited $n = 2$ levels of hydrogen (interacting with oxygen); this is due to the number of short-range non-adiabatic regions taken into account by the probability current approach using the *ab initio* potentials.

Our results were compared with other available data, in particular the recent rate coefficients calculated by Barklem (2018) by means of a multichannel approach based on asymptotic LCAO potentials. While a relatively good agreement is found for the largest rates, due to long-range ionic–covalent interaction, large differences up to several orders of magnitude are found for processes driven by short-range couplings.

Thus, the present study of O + H, $O^+ + H^-$ and $O^- + H^+$ collisions, based on accurate *ab initio* potentials and taking into account all non-adiabatic regions, results in high global accuracy of the calculated collision rates, higher than that of the previous data. The present rate coefficients are important, in particular for oxygen triplet modelling.

ACKNOWLEDGEMENTS

The authors acknowledge the referee for useful comments. AKB and YVV gratefully acknowledge support from the Ministry for Education and Science (Russian Federation), project Nos 3.5042.2017/6.7, 3.1738.2017/4.6. This work was partly supported by the French CNRS–PNPS (Programme National de Physique Stellaire), the GAIA program of Paris Observatory. Some of the *ab initio* quantum chemistry calculations were performed using HPC resources from GENCI-[CINES/IDRIS] (grant no. 2015047344) and on work stations at the Centre Informatique of Paris Observatory and at MSME laboratory (University of Paris-Est).

REFERENCES

Abrahamsson E., Krems R. V., Dalgarno A., 2007, ApJ, 654, 1171
Allende Prieto C., Asplund M., Fabiani Bendicho P., 2004, A&A, 423, 1109
Amarsi A. M., Barklem P. S., Asplund M., Collet R., Zatsarinny O., 2018, A&A, 616, A89

Barklem P. S., 2016, Phys. Rev. A, 93, 042705
Barklem P. S., 2017, Phys. Rev. A, 95, 069906(E)
Barklem P. S., 2018, A&A, 610, A57
Barklem P. S., Belyaev A. K., Guitou M., Feautrier N., Gadéa F. X., Spielfiedel A., 2011, A&A, 530, A94
Beames J. M., Liu F., Lester M. I., Murray C., 2011, J. Chem. Phys., 134, 241102
Belyaev A. K., 2013a, Phys. Rev. A, 88, 052704
Belyaev A. K., 2013b, A&A, 560, A60
Belyaev A. K., Barklem P. S., 2003, Phys. Rev. A, 68, 062703
Belyaev A. K., Lebedev O. V., 2011, Phys. Rev. A, 84, 014701
Belyaev A. K., Voronov Y. V., 2018, ApJ, 868, 86
Belyaev A. K., Yakovleva S. A., 2017, A&A, 606, A147
Belyaev A. K., Yakovleva S. A., 2018, MNRAS, 478, 3952
Belyaev A. K., Grosser J., Hahne J., Menzel T., 1999, Phys. Rev. A, 60, 2151
Belyaev A. K., Barklem P. S., Dickinson A. S., Gadéa F. X., 2010, Phys. Rev. A, 81, 032706
Belyaev A. K., Barklem P. S., Spielfiedel A., Guitou M., Feautrier N., Rodionov D. S., Vlasov D. V., 2012, Phys. Rev. A, 85, 032704
Belyaev A. K., Yakovleva S. A., Barklem P. S., 2014, A&A, 572, A103
Belyaev A. K., Voronov Y. V., Yakovleva S. A., Mitrushchenkov A., Guitou M., Feautrier N., 2017, ApJ, 851, 59
Belyaev A. K., Voronov Y. V., Gadéa F. X., 2018, ApJ, 867, 87
Berg D. A., Skillman E. D., Henry R. B. C., Erb D. K., Carigi L., 2016, ApJ, 827, 126
Bertran de Lis S. et al., 2016, A&A, 590, A74
Brewer J. M., Fischer D. A., 2016, ApJ, 831, 20
de Beer E., Koopmans M. P., de Lange C. A., Wang Y., Chupka W. A., 1991, J. Chem. Phys., 94, 7634
Drawin H. W., 1968, Zeitschrift für Physik, 211, 404
Drawin H. W., 1969, Zeitschrift für Physik, 225, 483
Easson I., Pryce H. L., 1973, Can. J. Phys., 51, 518
Federman S. R., Shipsey E. J., 1983, ApJ, 269, 791
Greenslade M. E., Lester M. I., Radenović D. Č., van Roij A. J. A., Parker D. H., 2005, J. Chem. Phys., 123, 074309
Guitou M., Belyaev A. K., Barklem P. S., Spielfiedel A., Feautrier N., 2011, J. Phys. B: Atomic Molecular Physics, 44, 035202
Guitou M., Spielfiedel A., Rodionov D. S., Yakovleva S. A., Belyaev A. K., Merle T., Thévenin F., Feautrier N., 2015, Chem. Phys., 462, 94
Krems R. V., Jamieson M. J., Dalgarno A., 2006, ApJ, 647, 1531
Li L., Nikiforov A., Xiong Q., Lu X., Taghizadeh L., Leys C., 2012, J. Phys. D: Appl. Phys., 45, 125201
Mitrushchenkov A., Guitou M., Belyaev A. K., Yakovleva S. A., Spielfiedel A., Feautrier N., 2017, J. Chem. Phys., 146, 014304
Mitrushchenkov A., Guitou M., Belyaev A. K., Voronov Y. V., Feautrier N., 2019, J. Chem. Phys., 150, 064312
Mitrushenkov A. O., 1994, Chem. Phys. Lett., 217, 559
Parlant G., Yarkony D. R., 1999, J. Chem. Phys., 110, 363
Pazira H., Kiselman D., Leenaarts J., 2017, A&A, 604, A49
Pereira T. M. D., Asplund M., Kiselman D., 2009, A&A, 508, 1403
Qin X., Zhang S. D., 2014, Journal of Korean Physical Society, 65, 2017
Sitnova T. M., Mashonkina L. I., 2018, Astron. Lett., 44, 411
Steenbock W., Holweger H., 1984, A&A, 130, 319
Steffen M., Prakapavičius D., Caffau E., Ludwig H.-G., Bonifacio P., Cayrel R., Kučinskas A., Livingston W. C., 2015, A&A, 583, A57
Stephens J. A., McKoy V., 1990, J. Chem. Phys., 93, 7863
van der Loo M. P. J., Groenenboom G. C., 2005, J. Chem. Phys., 123, 074310
van Dishoeck E. F., Langhoff S. R., Dalgarno A., 1983, J. Chem. Phys., 78, 4552
Wilson D. J., Gänsicke B. T., Farihi J., Koester D., 2016, MNRAS, 459, 3282
Yakovleva S. A., Voronov Y. V., Belyaev A. K., 2016, A&A, 593, A27
Yakovleva S. A., Barklem P. S., Belyaev A. K., 2018a, MNRAS, 473, 3810
Yakovleva S. A., Belyaev A. K., Kraemer W. P., 2018b, Chem. Phys., 515, 369
Yakovleva S. A., Belyaev A. K., Kraemer W. P., 2019, MNRAS, 483, 5105

SUPPORTING INFORMATION

Supplementary data are available at *MNRAS* online.

Supplementary data are presented in the files ReadMe.txt, rc_1000.dat, rc_2000.dat, rc_3000.dat, rc_4000.dat, rc_5000.dat, rc_6000.dat, rc_7000.dat, rc_8000.dat, rc_9000.dat, rc_10000.dat . The files *.dat contain rate coefficients in units of $cm^3\ s^{-1}$ for inelastic O + H, O^+ + H and O^- + H collisions for temperatures from $T = 1'000$ K to $T = 10'000$ K.

Please note: Oxford University Press is not responsible for the content or functionality of any supporting materials supplied by the authors. Any queries (other than missing material) should be directed to the corresponding author for the article.

APPENDIX A: STATISTICAL PROBABILITIES FOR SCATTERING CHANNELS

Table A1 presents the statistical probabilities for all scattering channels treated in the present work.

Table A1. $p_{\rm stat}$ for all scattering channels.

j	Asymptotic atomic states	$^4\Sigma^-$	$^2\Sigma^+$	$^2\Pi$	$^2\Sigma^-$	$^4\Pi$	$^6\Sigma^-$	$^2\Delta$	$^4\Delta$	$^6\Pi$	$^4\Sigma^+$
1	$O(2p^4\,^3P) + H(1s)$	4/18	–	4/18	2/18	8/18	–	–	–	–	–
2	$O(2p^4\,^1D) + H(1s)$	–	1/5	2/5	–	–	–	2/5	–	–	–
3	$O(2p^4\,^1S) + H(1s)$	–	1	–	–	–	–	–	–	–	–
4	$O(2p^3 3s\,^5S^o) + H(1s)$	4/10	–	–	–	–	6/10	–	–	–	–
5	$O(2p^3 3s\,^3S^o) + H(1s)$	4/6	–	–	2/6	–	–	–	–	–	–
6	$O(2p^4\,^3P) + H(2s)$	4/18	–	4/18	2/18	8/18	–	–	–	–	–
7	$O(2p^4\,^3P) + H(2p)$	4/54	2/54	4/54	2/54	8/54	–	4/54	8/54	–	4/54
		4/54	–	4/54	2/54	8/54	–	–	–	–	–
8	$O(2p^3 3p\,^5P) + H(1s)$	4/30	–	–	–	8/30	6/30	–	–	12/30	–
9	$O(2p^3 3p\,^3P) + H(1s)$	4/18	–	4/18	2/18	8/18	–	–	–	–	–
10	$O(2p^3 4s\,^5S^o) + H(1s)$	4/10	–	–	–	–	6/10	–	–	–	–
11	$O(2p^3 4s\,^3S^o) + H(1s)$	4/6	–	–	2/6	–	–	–	–	–	–
$i1$	$O^-(2p^5\,^2P) + H^+$	–	1/3	2/3	–	–	–	–	–	–	–
$i2$	$O^+(2p^3\,^4S^o) + H^-(^1S)$	1	–	–	–	–	–	–	–	–	–

This paper has been typeset from a TEX/LATEX file prepared by the author.